



EnergyPlus simulations of naturally ventilated buildings: comparison with validated CFD simulations

Simulaciones EnergyPlus de edificios con ventilación natural: Comparación con simulaciones CFD validadas

Cruz-Salas Miriam Verónica

Universidad Nacional Autónoma de México

Instituto de Energías Renovables

E-mail: mvcrs@ier.unam.mx

<https://orcid.org/0000-0002-6211-5263>

Huelsz Guadalupe

Universidad Nacional Autónoma de México

Instituto de Energías Renovables

E-mail: ghl@ier.unam.mx

<http://orcid.org/0000-0002-0624-0203>

Castillo José Antonio

Instituto Politécnico Nacional

Unidad Profesional Interdisciplinaria de Ingeniería

Campus Palenque, México

E-mail: jcastillot@ipn.mx

<https://orcid.org/0000-0003-0233-8075>

Abstract

EnergyPlus (EP) simulations using the Airflow Network model are performed for two types of natural ventilation, the cross ventilation (CV) and upward cross ventilation (UCV). The UCV is produced by a window and a windexchanger. Wind and thermal buoyancy effects are taken into account. The wind speed is varied and two buoyancy effect modes are tested: constant heat flux through the floor and constant floor temperature. Two alternative coefficient groups are used in the EP simulations. The first group includes the discharge coefficient taken from the literature and the pressure coefficients calculated by EP. In the second group, the coefficients are obtained from CFD simulations. EP simulation results of indoor air temperature and airflow rate are compared with those from validated CFD simulations. This research singles out the ranges of velocity and heat levels in which EP produces results in agreement with the CFD simulations and recommends the use of the EP cross-ventilation model for the CV and UCV configurations.

Keywords: Natural ventilation, airflow network model, cross ventilation, upward cross ventilation.

Resumen

Las simulaciones EnergyPlus (EP) utilizando el modelo Airflow Network se realizan para dos tipos de ventilación natural, la ventilación cruzada (CV) y la ventilación cruzada ascendente (UCV). El UCV está formado por una ventana y un intercambiador de viento. Se tienen en cuenta los efectos del viento y la flotabilidad térmica. Se varía la velocidad del viento y se prueban dos modos de efecto de flotabilidad: Flujo de calor constante a través del suelo y temperatura constante del suelo. En las simulaciones de EP se utilizan dos grupos de coeficientes alternativos. El primer grupo incluye el coeficiente de descarga tomado de la literatura y los coeficientes de presión calculados por EP. En el segundo grupo, los coeficientes se obtienen a partir de simulaciones CFD. Los resultados de la simulación EP de la temperatura del aire interior y el caudal de aire se comparan con los de simulaciones CFD validadas. Esta investigación destaca los rangos de velocidad y niveles de calor en los que EP produce resultados de acuerdo con las simulaciones CFD.

Descriptores: Ventilación natural, modelo de red de flujo de aire, ventilación cruzada, ventilación cruzada ascendente.

INTRODUCTION

Natural ventilation (NV) in buildings can cut fan and cooling energy use, improving indoor air quality and occupant comfort during hot seasons. Architects and engineers increasingly rely on thermal building simulations for design and retrofitting, making accurate NV simulations crucial.

Building thermal and energy performance simulation encompasses physical models, statistical techniques, and hybrid models (Fouquier *et al.*, 2013). Physical models analyze the thermal and energy performance of a specific building. Statistical methods assess energy performance for specific building types in particular areas. Physical models are further categorized into computational fluid dynamics (CFD), zonal, and multizone (nodal) approaches. CFD provides three-dimensional air temperature and velocity insights but is time-intensive for year-long whole-building simulations. Zonal modeling offers two-dimensional air temperature and velocity data and suits large space buildings (Lu *et al.*, 2020). Multizone (nodal) modeling treats each building zone as a uniform entity, making it suitable for year-long whole-building simulations.

Multizone building thermal and energy simulation software, like EnergyPlus (EP), incorporates the multizone Airflow Network model (AFN) to simulate natural or mechanical ventilation (ASHRAE, 2013). AFN comprises interconnected nodes and airflow components, where node variables represent pressure and linkage variables denote airflow rates. AFN of EP (EP-AFN) operates through three sequential stages: pressure and airflow computations, node temperature and humidity evaluations, and sensible and latent load assessments (DOE, 2016). EP offers two additional ventilation models alongside the AFN: the Design Flow Rate and the Wind and Stack Open Area models (DOE, 2016). The first model may not replicate realistic conditions for NV since it relies on a predetermined flow rate. The second model is tailored for NV but has a notable drawback. It calculates the flow rate based on wind speed, thermal buoyancy, area, and the discharge coefficient (C_d) of the opening, without considering the presence of other openings in the thermal zone. This omission can lead to inaccuracies in results.

EP provides various room air models, with the Cross Ventilation model being the only one that furnishes air velocity data for three distinct regions within the thermal zone (the jet, recirculation, and window jet).

In EP-AFN, input parameters include the wind pressure coefficient (C_p) for each external node and the discharge coefficient (C_d) for each opening. Additiona-

lly, the opening factor, representing the fraction of the opening allowing airflow, must be specified for each opening (DOE, 2016).

There are several studies that report EP simulations using natural, mechanical, or mixed-mode ventilation, but relatively few of them explicitly report the use of the AFN.

EP-AFN has been applied to mechanically ventilated buildings (Rusly & Piechowski, 2011; Yan *et al.*, 2015; Cheng *et al.*, 2017), to double skin facades of air-conditioned buildings (Chan *et al.*, 2009; Hashemi *et al.*, 2010; Choi *et al.*, 2012; Joe *et al.*, 2013; Sung *et al.*, 2013; Le *et al.*, 2014; Peng *et al.*, 2016; Anđelković *et al.*, 2016), and to air-conditioned buildings that employ natural night ventilation for energy saving purpose (Ramponi *et al.*, 2014; Albuquerque *et al.*, 2020).

EP-AFN has also been applied in naturally ventilated buildings (Zhai *et al.*, 2011; Zhang *et al.*, 2013; Schulze & Eicker, 2013; Belleri *et al.*, 2014; Arendt *et al.*, 2017; Gimenez *et al.*, 2018; Shirzadi *et al.*, 2018; Dogan & Kastner, 2021; Goncalves *et al.*, 2022; Chu, 2023; Li & Chen, 2023; Salvati & Kolokotroni, 2023; Yin & Muhieldeen, 2024). Most of these studies assessed the accuracy of EP-AFN in specific building context (Zhai *et al.*, 2011; Zhang *et al.*, 2013; Belleri *et al.*, 2014; Arendt *et al.*, 2017; Gimenez *et al.*, 2018; Goncalves *et al.*, 2022; Li & Chen, 2023; Chu, 2023; Salvati & Kolokotroni, 2023; Yin & Muhieldeen, 2024). Other studies considered generic cross-ventilation cases solely with the wind effect (Shirzadi *et al.*, 2018; Chu, 2023). Other authors studied the impact of the wind pressure coefficient on the ventilation building (Xie *et al.*, 2023; Sakiyama *et al.*, 2024). Some investigations compared simulation outcomes to field measurements (Zhai *et al.*, 2011; Belleri *et al.*, 2014; Arendt *et al.*, 2017; Shirzadi *et al.*, 2018), focusing on parameters like the indoor air temperature (T_i) (Zhai *et al.*, 2011; Belleri *et al.*, 2014; Arendt *et al.*, 2017) and the ventilation flow rate (Q) (Zhang *et al.*, 2013; Belleri *et al.*, 2014; Arendt *et al.*, 2017; Shirzadi *et al.*, 2018). Also, the air changes per hour (A_{CH}) and the annual cooling degree hours have been employed as parameters (Gimenez *et al.*, 2018). Certain studies enhance accuracy by coupling EP (Zhang *et al.*, 2013; Goncalves *et al.*, 2022) or other multi-zone programs (Tan & Glicksman, 2005; Ohba & Lun, 2010) with CFD simulations, though this approach may pose challenges in buildings with numerous zones. A gap exists in assessing the accuracy of models in EP-AFN for generic naturally ventilated buildings that incorporate both wind and buoyancy effects. This study aims to address this gap by evaluating the precision of EP-AFN simulations through a comparison with CFD simulations. Specifically, it examines two natural ventilation configurations: cross ventilation and

upward cross ventilation, within a generic isolated building. The analysis accounts for wind and buoyancy effects, with variations in wind speed and heating. Two heating modes are considered: internal heat gains and floor temperature.

In this study, CFD simulations serve as a reference for evaluating EP-AFN results. To ensure the credibility of CFD simulations, they have undergone validation against experimental data. In the literature, numerous studies validate CFD simulations for natural ventilation cases, primarily focusing on wind effects. Some examples of these validations are (Castillo & Huelsz, 2017; Kobayashi *et al.*, 2022; Kumar *et al.*, 2021; Zheng *et al.*, 2020; Castillo *et al.*, 2019; Kosutova *et al.*, 2019; van Hooff *et al.*, 2017; van Hooff & Blocken, 2010; Peren *et al.*, 2015; Perén *et al.*, 2015; Ramponi & Blocken, 2012). However, there are fewer reports validating CFD simulations for cases involving thermal buoyancy effects (Kosutova *et al.*, 2018; Gilani *et al.*, 2016). The CFD simulations presented in this paper are validated with experimental studies that consider the wind effect (Kurabuchi *et al.*, 2004; Cruz-Salas *et al.*, 2014) and another one that considers both effects (Lishman & Woods, 2006).

STUDY CASES

The natural ventilation, in steady state, of a generic isolated building is considered. The fixed parameters for all cases are: outdoor air temperature and relative humidity, atmospheric pressure, wind profile and direction, and no radiative heat exchanges. The walls and roofs are considered adiabatic. The fact of neglecting the solar radiation effect makes the case more generic. The consideration of adiabatic walls and roofs increases the ventilation effect, which is the purpose of the present study, and this condition is close to the highly insulated envelopes.

Two configurations are analyzed: cross ventilation (CV) and upward cross ventilation (UCV). In the CV configuration, the building has two axial opposite windows at the center of the wall, one at windward and the other one at leeward. In the UCV the building has a window at windward and one windexchanger (WE) (Cruz-Salas *et al.*, 2014; Castillo *et al.*, 2017) on the roof with a single opening at leeward. Thus, the WE opening is at a higher level than that of the window.

Building geometries for both configurations are shown in Figure 1. In the CV configuration, the building has an internal area of 4.20 m × 4.20 m and an internal height of 2.10 m, with two opposite windows of 0.90 m × 0.45 m. The building roof is flat. This geometry was taken from (Kurabuchi *et al.*, 2004). In the UCV configuration, the building has an internal area of 3.0 m × 3.0 m and an

internal height of 2.7 m. The window is square with a side length of 1.30 m, it is horizontally centered on the wall and its base is at 0.90 m from the floor. The WE is at the center of the building roof, it has a square cross-section duct with an internal side length of 0.65 m, and an internal height of 1.40 m when measured from the rooftop. The WE has a single square opening area equal to that of the WE duct cross-section. The building and the WE roof are flat. This building geometry was taken from the COLW case of (Castillo *et al.*, 2017).

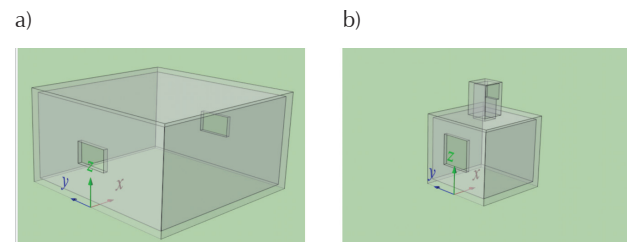


Figure 1. Building geometry for both configurations: a) cross ventilation (CV) and b) upward cross ventilation (UCV)

Two heating modes are considered for the CV and UCV configurations. Each one of these has four heating levels. One mode sets the rate of heat flow through the floor (q) (H cases), with values: 0 W, 250 W, 500 W and 750 W. The other mode sets the floor temperature (T cases), with values: 15 °C, 25 °C, 35 °C and 45 °C. Therefore, there are four groups of cases: CV-H, UCV-H, CV-T and UCV-T. Additionally, the wind speed at a 10 m height (v_{10}) varies along five values: 0.1 m/s, 0.5 m/s, 1 m/s, 3 m/s, and 5 m/s. Thus, a total of 80 study cases are tested.

CFD SIMULATIONS

Three dimensional simulations are performed with the commercial CFD code ANSYS Fluent 19 (ANSYS, 2018).

GENERAL SETTINGS AND PARAMETERS

For all simulations, the grids are generated with the surface cell extrusion technique, obtaining a block structured grid with hexahedral cells (van Hooff & Blocken, 2010). The height of the first cell extrusion $z_1 = 2.1 k_s = 0.002$ m is calculated according to Castillo *et al.* (2019). A grid growing factor of 20 % is used. The domain dimensions are set according to the guidelines given by Franke *et al.* (2007) and Tominaga *et al.* (2008). Three grids are generated for the grid sensitivity analysis. The course grid and the fine grid are built multiplying each spatial coordinate of the base grid by $(1/2)^{1/3}$ and $2^{1/3}$, respectively. The steady RANS equations are solved with the SIMPLEC algorithm for pressure and

velocity coupling using a second order upwind scheme. Second order discretization schemes are used for the convection and the viscous terms of the governing equations (Ramponi & Blocken, 2012). 10,000 iterations are set as the stopping criteria. Convergence is considered to have been reached if the scaled residuals are less than 10^{-5} . The inlet boundary condition for the velocity profile is the logarithmic law $U(z) = (u_{ABL}^*/\kappa)\ln((z + z_0)/z_0)$, where u_{ABL}^* [m/s] is the atmospheric boundary layer friction velocity, $\kappa = 0.42$ [-] is the von Karman constant, z_0 [m] is the roughness length and z [m] is the height coordinate. The turbulent profiles are: the turbulent kinetic energy $k(z)$, the turbulence dissipation rate $\varepsilon(z)$, and the specific dissipation rate $\omega(z)$. These profiles are calculated using the following equations: $k(z) = \sigma_u^2(z)$, $\varepsilon(z) = u_{ABL}^{*3}/\kappa(z + z_0)$ and $\omega(z) = \varepsilon(z)/C_\mu k(z)$. Where σ_u [m²/s²] is the standard deviation of the velocity in the x direction and $C_\mu = 0.09$ [-] is an empirical constant (Tominaga *et al.*, 2008). The standard wall functions with roughness modification (Cebeci & Bradshaw, 1977) are set on the ground surface. The values of the sand grain roughness height $k_s = 9.793z_0/C_s$ [m] and the roughness constant C_s [-] are calculated according to Blocken *et al.* (2007). For the building surfaces, standard wall functions are set with zero roughness height ($k_s = 0$). Zero static pressure is applied at the domain outlet. Depending on the validation case, different boundary conditions are set at the top and lateral sides of the domain.

VALIDATION OF WIND-DRIVEN CROSS VENTILATION

Experimental results of a wind-driven CV case (Figure 2a, b) obtained in a wind tunnel using particle image velocimetry (PIV) by Kurabuchi *et al.* (2004) are used for the CFD validation. This validation has been presented in detail by the authors in (Castillo & Huelsz, 2017).

In the CFD simulations, the values of $u_{ABL}^* = 0.75$ m/s and $z_0 = 0.0027$ m are used to reproduce the inlet velocity profile. The $k_s = 0.0039$ m is used in the roughness modification equation (Cebeci & Bradshaw, 1977). Symmetry condition is applied at the top and lateral si-

des of the domain. Streamwise gradient analyses are done for velocity as well as for turbulence parameters (Blocken *et al.*, 2007). Figure 2c shows the streamwise gradients which are lower than 3 %.

Figure 3a shows a small grid sensitivity along the center line L_r (base grid has 1,448,712 cells). The average difference of the u/U_{ref} between the coarse and base grids is around 7 %, while the average difference between the base and fine grids is lower than 2 %. The reference velocity, U_{ref} is the wind velocity at the building height. Figure 3b presents the impact of three turbulence models (SST $k-\omega$, Rk- ε and RNG $k-\varepsilon$) on u/U_{ref} . The average difference of u/U_{ref} along L_r , between the experimental and CFD results obtained using the base grid and the SST $k-\omega$ turbulence model is lower than 10 %. The velocity vector field at the central plane shows a close qualitative agreement between experimental and CFD results (Figures 3c). From these results, CFD simulations for the wind driven CV case are considered as validated.

VALIDATION OF WIND DRIVEN UPWARD CROSS VENTILATION

Experimental results of a wind driven UCV case (Figure 4a, b) obtained using an open water channel (OWC) and stereoscopic particle image velocimetry (SPIV) (Cruz-Salas *et al.*, 2014) are used for the CFD validation. The validation was performed following the methodology in (Castillo *et al.*, 2019), because the UCV case is similar to the case validated in that work.

In the CFD simulation, the computational domain (base grid with 1,837,108 cells) is constructed to reproduce the OWC test section. This domain has a deviation from the guidelines (Franke *et al.*, 2007; Tominaga *et al.*, 2008), but it is required in order to reproduce the narrow width of the OWC. The values of $u_{ABL}^* = 0.007$ m/s and $z_0 = 0.0006$ m are used for the velocity profile and $k_s = 0.002$ m is used in the roughness modification equation. Free slip condition (Gallardo *et al.*, 2013) is applied at the top. The lateral walls are specified as smooth no slip walls. In Figure 4c, the streamwise gradients of the U

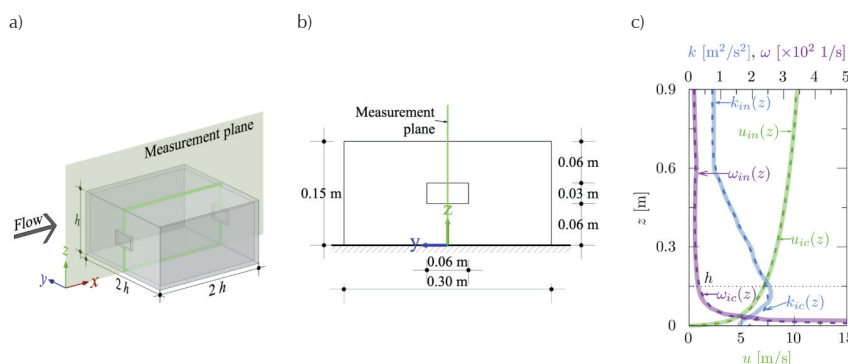


Figure 2. Wind driven cross ventilation case for validation: a) scaled model isometric view with measurement plane, b) scaled model front view with dimensions and c) vertical profiles of the air velocity, u ; turbulent kinetic energy, k , and the specific dissipation rate, ω , at the inlet (solid line) and at the incident position (dashed line) in the empty domain. The subscripts *in* and *ic* refer to inlet and incident, respectively. Data from Kurabuchi *et al.* (2004)

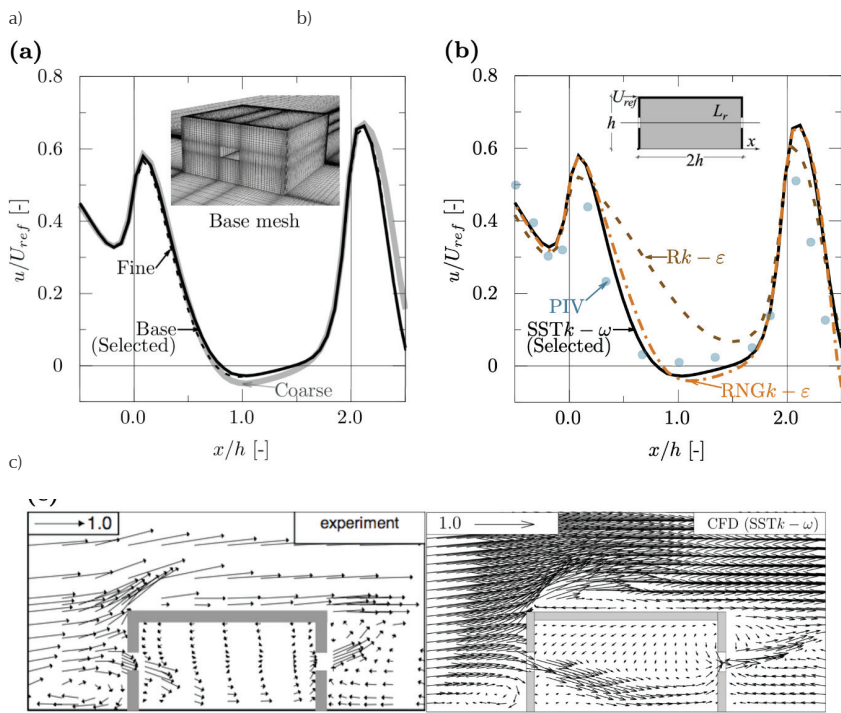


Figure 3. Wind driven cross ventilation case for validation: a) grid sensitivity analysis comparing the normalized air velocity u/U_{ref} along the center line L_r , b) sensitivity analysis of the impact of turbulence models (SST $k-\omega$, Rk- ϵ and RNG $k-\epsilon$) compared with PIV measurements; and c) velocity vector fields for the vertical central plane from experiments and CFD simulations using the SST $k-\omega$ turbulence model. Data from Kurabuchi *et al.* (2004)

and ω profiles are below 3 %. However, the k profile shows a large difference when close to the floor, similar to the one found in other natural ventilation simulations (Blocken *et al.*, 2007; Ramponi & Blocken, 2012; Blocken, 2015).

In Figure 5a, u/U_{ref} along L_r is presented. The average difference for u/U_{ref} between the coarse and base grids is around 3 %, while the difference between the base and fine grids is lower than 1 %. Compared to the experimental results (Figure 5b), the SST $k-\omega$ and RNG $k-\epsilon$ models have an averaged error below 10 %, while

the R $k-\epsilon$ has a larger value. The comparison of u/U_{ref} between numerical and experimental results has an average error below 10 %. Thus, the wind driven UCV simulations are considered as validated. For the CFD simulation results presented the Results section, the domain for the UWV configuration is reconstructed in strict adherence to the guidelines (Franke *et al.*, 2007; Tominaga *et al.*, 2008; Blocken, 2015).

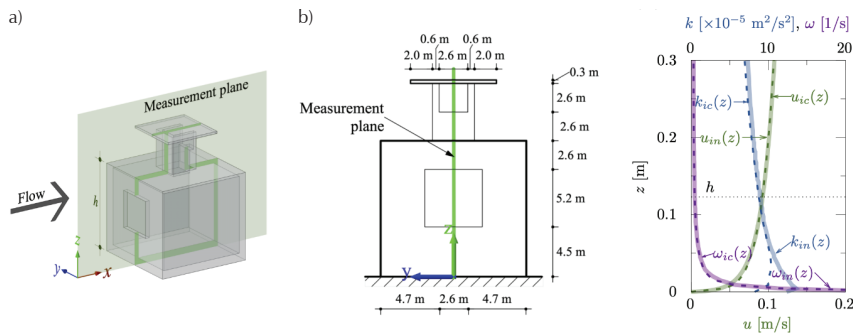


Figure 4. Wind driven upward cross ventilation case for validation: a) scaled model isometric view with measurement plane, b) scale model front view with dimensions, and c) vertical profiles of the fluid velocity, u ; turbulent kinetic energy, k , and the specific dissipation rate, ω , at the inlet (solid line) and at the incident position (dashed line) in the empty domain. The subscripts *in* and *ic* refer to inlet and incident, respectively

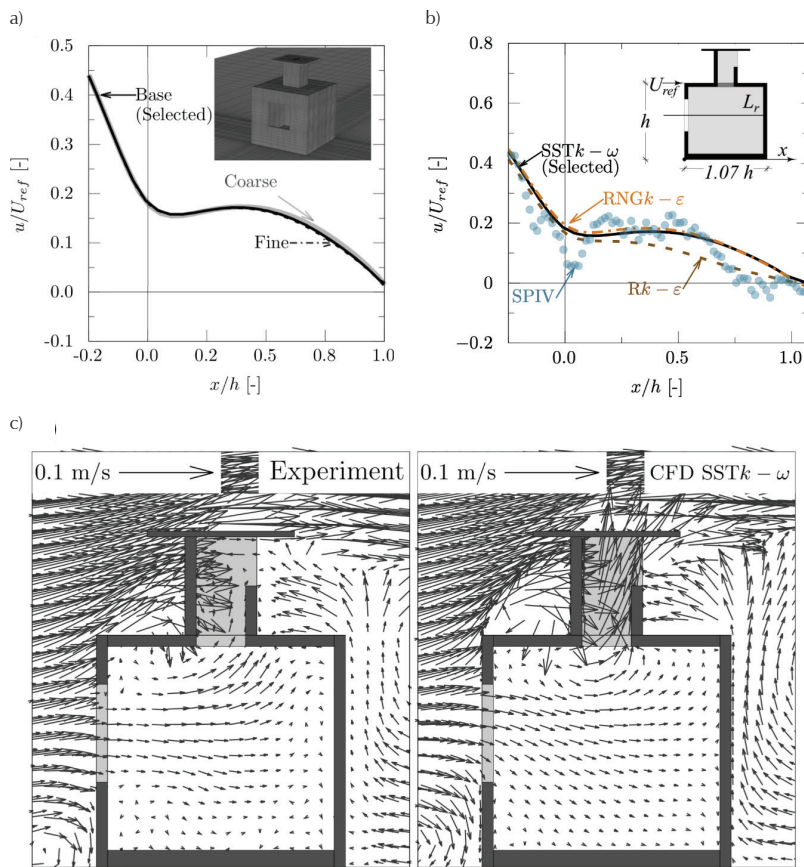


Figure 5. Wind driven upward cross ventilation case for validation: a) grid sensitivity analysis comparing the normalized air velocity u/U_{ref} along the center line L_r , b) sensitivity analysis of the impact of turbulence models (SST $k-\omega$, Rk- ϵ and RNG $k-\epsilon$) compared with SPIV measurements (Cruz-Salas *et al.*, 2014), and c) velocity vector fields for the vertical central plane from experiments (Data from Cruz-Salas *et al.* (2014) and CFD simulations using the SST $k-\omega$ turbulence model

VALIDATION OF WIND AND BUOYANCY DRIVEN UPWARD CROSS VENTILATION

Experimental results of a case with the UCV configuration considering wind and buoyancy effects reported in (Lishman & Woods, 2006) are used for the CFD validation. The experiments employed water in a flume and thermocouple measurements (Figure 6a, b). The validity of the ventilation experiments using water is given in terms of the fact that the laboratory model and the real building have geometric, kinematic, and dynamic similarity. This validation is presented in more detail than the previous ones since it is the first time it is being reported. Lishman & Woods (2006) used a scaled model of a building with circular openings, 7 at the top in the windward facade and 7 at the bottom in the leeward facade. The flume had a transversal section area of 0.5 m \times 0.5 m. The heat was supplied from the model floor by a heating plate with a series of high resistance metal coils. Five values of the heat flow rate q were tested (0 W, 11 W, 42 W, 76 W, 120 W). The temperature was measured using 4 thermocouples vertically distributed within the interior of the model. The thermocouples had an uncertainty of ± 0.1 .

For the CFD simulations, the physical properties of the fluid are obtained from (Lishman & Woods, 2006). The Boussinesq approximation is used. In the convergence criteria the scaled residuals for energy are equal to 10^{-7} . The computational domain is constructed to reproduce the flume test section (Figure 6c). This domain also has a deviation from the guidelines (Franke *et al.*, 2007; Tominaga *et al.*, 2008). Three grids with hexahedral cells are generated (Figure 7a): the coarse grid has 270,079 cells; the base grid has 576,628 cells and the fine grid has 1,074,406 cells. Constant values of u and the turbulence intensity are set at the domain inlet (0.01 m/s and 0.1, respectively). Free slip condition (Gallardo *et al.*, 2013) is set at the domain top. The lateral walls of the domain are specified as smooth no slip walls. q is applied as a constant heat flux on the building floor. In Figure 7a the streamwise gradients of the u , k and ω profiles are presented. Their values are smaller than 6%.

In Figure 8 u/U_{ref} along a horizontal line (located in full scale at 1.7 m above the floor) and a sloped line are presented. For both lines of interest, the average difference of u/U_{ref} between the coarse and base grids is lower than 7%, while the difference between the base and fine grids is lower than 6%. Therefore, the base grid is selected.

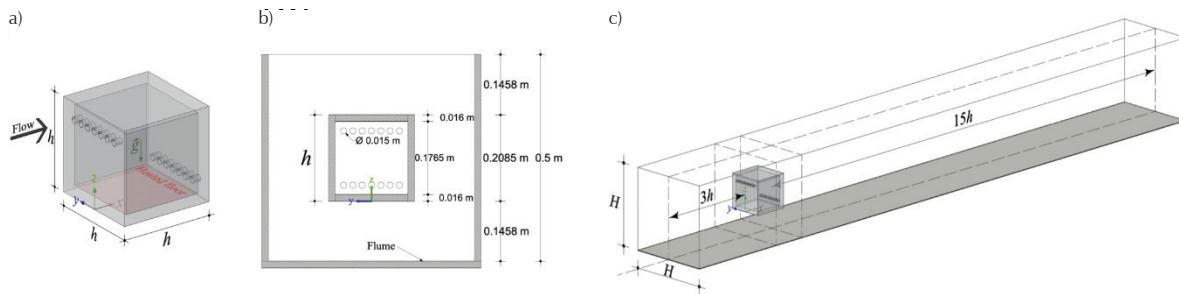


Figure 6. Scaled model of a building with circular top openings at its windward facade and bottom openings at its leeward facade: a) right isometric view, b) front view with dimensions and c) isometric view of the computational domain with dimensions. $h = 0.2085$ m is the characteristic length

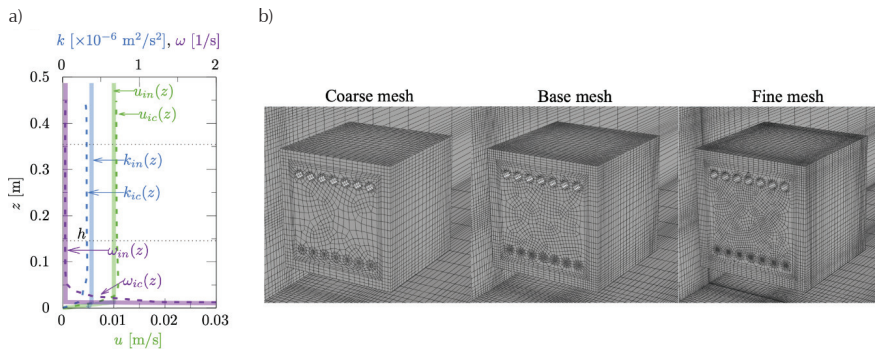


Figure 7. Wind and buoyancy driven upward cross ventilation case for CFD validation: a) streamwise gradients of the fluid x-component velocity, u , the turbulent kinetic energy, k , and the specific dissipation rate, ω , at the inlet (solid line) and at the incident position (dashed line) in the empty domain. The subscripts in and ic refer to inlet and incident, respectively. And b) isometric view of three grids of the model: coarse, base and fine

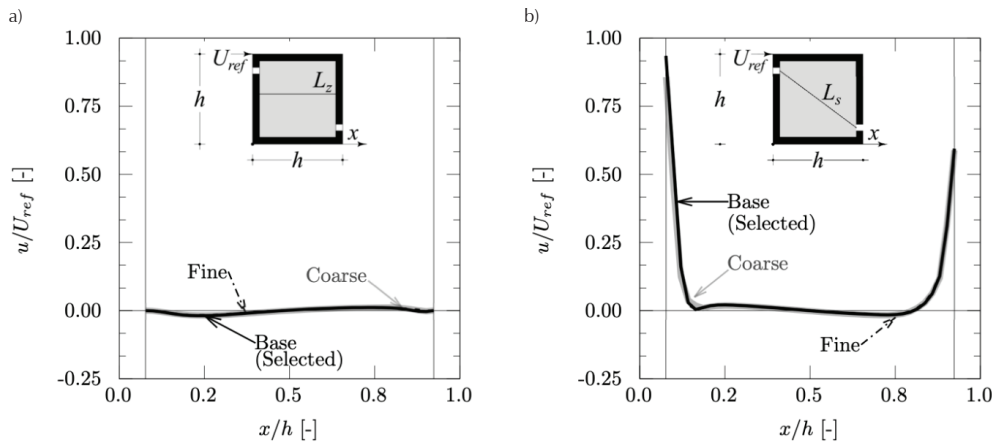


Figure 8. Grid sensitivity analysis of the normalized air velocity u/U_{ref} along: a) horizontal line (in full scale at 1.7 m above the floor) L_z and b) a sloped line L_s

The temperature difference between the indoor and outdoor fluid ΔT from three turbulence models (SST $k-\omega$, R $k-\epsilon$ and RNG $k-\epsilon$) is compared to the experimental results from (Lishman & Woods, 2006). The results for different values of q are shown in Table 1. For all values of q , the average of the absolute difference of ΔT

between the turbulence model and the experiment is 0.3°C for SST $k-\omega$ and RNG $k-\epsilon$, while for R $k-\epsilon$ is 0.4°C . Therefore, the three turbulence models are suitable for this UCV case. The SST $k-\omega$ model is selected for further simulations because this turbulence model is also accurate in the CV and UCV cases that only consider

wind effect. Thus, the simulations of the UCV configuration with wind and buoyancy effects are validated. The parameters and settings of this section are applied to the simulation reported in the Results and discussion section.

Table 1. Heat flow rate q and temperature absolute difference between the indoor and outdoor fluids ΔT . The data are obtained from experiments (Lishman & Woods, 2006) and from CFD simulations with three different turbulence models: SST $k-\omega$, RNG $k-\epsilon$ and $Rk-\epsilon$

q [W]	ΔT [°C]			
	Experiment	SST $k-\omega$	RNG $k-\epsilon$	$Rk-\epsilon$
11	0.1	0.4	0.4	0.6
42	0.4	0.8	0.7	1.0
76	0.9	1.1	1.0	1.3
120	1.7	1.3	1.3	1.6

OBTAINING OPENING COEFFICIENTS

The pressure coefficient C_p is a dimensionless parameter that is the difference between the local pressure and the reference pressure divided by the reference dynamic pressure, given by

$$C_p = \frac{p - p_{ref}}{\frac{1}{2} \rho_{ref} u_{ref}^2} \quad (1)$$

where p [Pa] is the local pressure, p_{ref} [Pa] is the static pressure in the freestream, ρ_{ref} [kg/m³] is the freestream fluid density and u_{ref} is a reference velocity. EP uses the freestream velocity at the midheight of the opening as the reference velocity.

In the CFD simulations the value of C_p for an opening is obtained with the area weighted average (ANSYS, 2018).

The airflow rate Q [m³/s] is calculated as the total inflow through all openings.

The discharge coefficient C_d is a characteristic parameter of an opening. It is the result of the contraction and friction of the flow and depends on the opening geometry (Karava *et al.*, 2004). For each opening functioning as entrance, C_d is calculated using:

$$C_d = \frac{Q_j}{u_{ref} A_j} \quad (2)$$

where Q_j is the inflow and A_j the area of the opening.

ENERGYPLUS SIMULATIONS SETTINGS

The geometry of each configuration is modeled with Sketchup 2017. A single thermal zone is considered for both configurations. In order to simulate the walls and roofs as adiabatic, they are considered as being made from 15 cm thick expanded polystyrene with the Outside Boundary Condition set as Adiabatic. In EP an opening cannot be defined within an adiabatic surface. Therefore, for any wall with an opening, a 5 cm wide frame around the opening is considered. The Outside Boundary Condition of this frame is set as Outdoors. Constructions thermal absorptance and the ground reflectance are set equal to 0.0001 in order to simulate a nonradiative heat exchange condition.

For the H cases the heat flux through the floor is set using ZoneHVACRadiant:Electric. Additional simulations are performed using the same heat flux while considering that the heat flux is produced by people (sensible heat). The results are the same for both types of heat sources. For T cases, the floor is set as Ground and it is considered to be made of steel with a thickness of 0.001 m.

To create a steady state, the object SizingPeriod: DesignDay can be used (Schulze & Eicker 2013). This can also be achieved by modifying the weather file. In this study, the latter procedure is employed. Five weather files, one for each wind speed value, are created using the Weather Statistics and Conversions of EP. Each weather file has constant values for all variables. In all files, the outdoor air temperature $T_o = 15$ °C, the atmospheric pressure is 1 atm, the relative humidity is 11 % (this is used to achieve the same air density considered in the CFD simulations), the solar radiation is zero and the wind direction is 0°. In EP, the radiative heat exchange to the sky is eliminated by setting the sky temperature as equal to T_o . The atmospheric boundary layer considered is that of a semi-urban area with a wind speed profile exponent of 0.25 and a 395 m thickness. The value of T_o is considered to be independent from the height.

The conduction transfer function algorithm is used. Since the simulations are in steady state, both the use of the input object Material:NoMass and that of the input object Material produce the same results. The Cross Ventilation model is used as the room air model. This model distinguishes two types of regions inside the building: main jet and recirculation. EP assesses whether the cross-ventilation model applies or not. If it does, EP uses this model, if it does not, EP uses the Mixing model. The TARP algorithm was used to model internal convection because it showed the best results in (Zhang *et al.*, 2013).

The simulations are made using two groups of coefficients in EP-AFN. In the first group (C1), the discharge coefficient for openings at windward is set equal to the value often assumed in the literature for a large opening functioning as an entrance ($C_{d-It} = 0.6$) (Heiselberg *et al.*, 2001). The pressure coefficient is set equal the one calculated by EP (C_{p-EP}) for each wall and roof of the building as a function of wind direction, building height, and footprint aspect ratio. In the second group (C2), the coefficients are obtained from the CFD simulations (C_{d-CFD} , C_{p-CFD}), as described in the section obtaining opening coefficients. The values for these coefficients are shown in Table 2. The existence of $C_p > 1.0$ values is due to the fact that the C_p obtained from CFD simulations are calculated in accordance to the EP consideration, *i.e.* the use of freestream velocity at mid-height of the opening as the reference velocity. In EP the maximum value of C_p accepted for windward openings is 1. Therefore, the input values of C_{p-CFD} used in EP were set by EP as 1. For C1 and C2, the value of C_d is set as 1.0 (Linden *et al.*, 1990) for all leeward openings. All openings are set as Detailed Opening. It was found

that the use of the Simple Opening type produces errors when the temperature difference in the zone is zero. The airflow rate, Q [m^3/s], is calculated as the sum of the inlet flow through all openings.

RESULTS AND DISCUSSION

Figure 9 shows temperature contour plots at the vertical central plane and on the floor for the CV and UCV configurations. These results are obtained for T cases with $v_{10} = 0.01$ m/s and a floor temperature of 45°C. For both configurations the highest indoor air temperature is close to the floor, forming a ring. As expected, the lowest temperature is at the incoming jet from the windward window. For the CV configuration, the temperature is around 27°C at the central vertical plane. The same temperature is found at the central zone close to the floor. For the UCV configuration, the temperature is around 17°C at the central vertical plane and around 22°C at the central zone close to the floor. The average indoor air temperatures of the CV and UCV are 27°C and 19°C, respectively.

Table 2. Coefficients considered in C1 and C2. Discharge coefficients and pressure coefficients for openings at windward (ww) and leeward (lw), for the two configurations and for the wind speed at a 10 m height (v_{10})

Configuration	v_{10} [m/s]	C1			C2		
		C_{d-It} [-]	C_{p-EP} [-]		C_{d-CFD} [-]	C_{p-CFD} [-]	
			ww	ww		lw	ww
CV	0.1	0.60	0.60	-0.36	0.51	1.21	-0.22
	0.5	0.60	0.60	-0.36	0.52	1.24	-0.20
	≥ 1	0.60	0.60	-0.36	0.52	1.04	-0.17
UCV	0.1	0.60	0.60	-0.36	0.16	1.22	-0.37
	0.5	0.60	0.60	-0.36	0.16	1.22	-0.34
	≥ 1	0.60	0.60	-0.36	0.15	1.13	-0.43

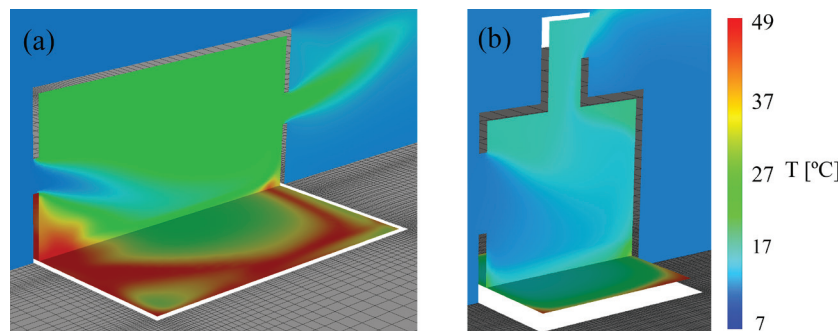


Figure 9. Temperature contour plots at the vertical central plane and on the floor, for T cases with $v_{10} = 0.01$ m/s and floor temperature of 45°C, a) cross ventilation and b) upward cross ventilation configurations

Results of the EP simulations using the coefficient groups C1 and C2 are compared with the results from the CFD simulations. Two comparison parameters are used: ΔT and Q .

Due to the configuration of the cases, the cross-ventilation model is set as the room air model for all cases. Additionally, this model is the only one that solves the air velocity within the thermal zone.

Nevertheless, EP does not apply this model for all cases. In general, EP applies the cross-ventilation model for high wind velocity and low heat level.

In the cases in which EP applied the cross-ventilation model, the maximum temperature difference between the recirculation and the jet was 0.3°C , shown by the UCV-T cases with $v_{10} = 3.0 \text{ m/s}$ and 35°C , and the cases with $v_{10} = 5.0 \text{ m/s}$ and 45°C . As expected, the recirculation region temperature is greater than the jet region temperature for cases with heating levels different from zero. The percentage velocity difference between the jet region and the recirculation region with respect to the jet region is up to 40 % for the CV cases and up to 42 % for the UCV cases.

The mixing model was tested for the cases where EP applied the CV model. The internal temperature calculated with both models is similar. The difference is less than 0.1°C .

Figures 10 to 13 show the comparison between EP and CFD simulations. In Figures 10 and 11 the comparison variable is ΔT , and in Figure 12 and Figure 13 the comparison variable is Q . In each graph, twenty cases are reported, corresponding to the five values of v_{10} and the four heat levels. The five values of v_{10} are identified with different symbols and colors. For a given v_{10} the four heat levels can be distinguished since the values of ΔT and Q increase with the increase of the heat flux or that of the temperature on the floor.

In the following paragraphs, when a pair of percentages is reported, the two results correspond to the C1 and C2 coefficient groups, respectively.

For CV-H cases (Figure 10) EP reproduces the CFD value of ΔT for $v_{10} \geq 1.0 \text{ m/s}$ with a difference of less than 5 % and 4 %, for $v_{10} = 0.5 \text{ m/s}$ the difference is of less than 26 % and 24 %, but for $v_{10} = 0.1 \text{ m/s}$ the difference is of up to 86 % and 85 %.

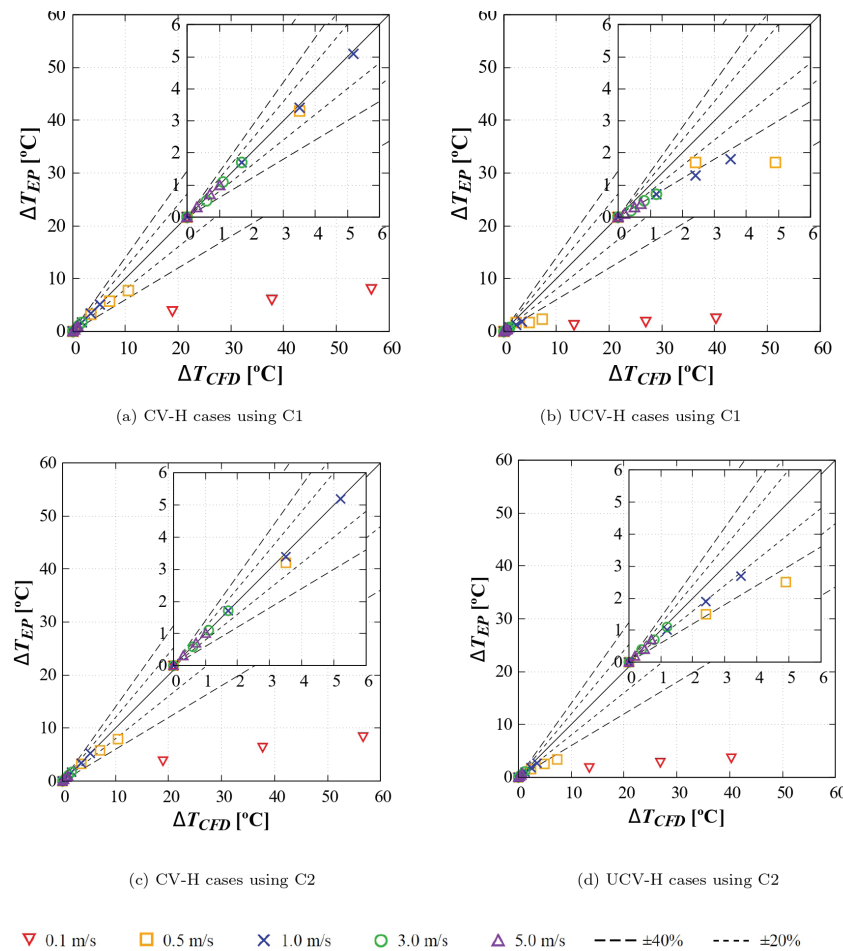


Figure 10. Comparison of ΔT from EnergyPlus and CFD simulations for H cases, and for different wind speeds and heat levels, a) and b) using C1, c) and d) using C2. Low values are enlarged in the insert. Symbols denote the wind speed at a 10 m height. For a given v_{10} the four heat levels can be distinguished since the values of ΔT and Q increase with the increase of the heat flux or the temperature on the floor. The dashed lines indicate the percentage error

For UCV-H cases, the difference between EP and CFD ΔT results for $v_{10} \geq 3.0$ m/s is of less than 38 % and 8 %, for $v_{10} = 1.0$ m/s the difference is of up to 48 % and 23 %, while for $v_{10} \leq 0.5$ m/s the difference is of up to 94 % and 91 %. For both configurations (CV and UCV) using C2 gives better results. Nevertheless, for CV-H cases the improvement is not significant. For UCV-H cases, especially for $v_{10} \geq 1.0$ m/s, the enhancement is significant.

In H cases, EP has a better agreement with CFD for the CV configuration than it does for the UCV configuration. For both configurations the agreement increases as v_{10} increases.

For CV-T cases, shown in Figure 11, EP reproduces the CFD value of ΔT for $v_{10} = 0.1$ m/s with a difference of less than 9 % and 11 %, and for $v_{10} = 3.0$ m/s with a difference of less than 29 % and 28 %, for the other values of v_{10} the difference is up to 62 % and 64 %. For UCV-T cases, the difference between EP and CFD ΔT results for $v_{10} = 0.1$ m/s is less than 10 % and 40 %, and for $v_{10} = 3.0$ m/s is less than 45 % and 20 %. For the other values of

v_{10} the difference is up to 64 % and 100 %. For CV-T cases the difference between C1 and C2 results is not significant, while for the UCV-T cases the difference is significant.

In T cases, EP has a similar agreement with CFD for both configurations. In both configurations the results do not show a tendency with respect to v_{10} .

When comparing the H and T cases using ΔT , in general, the agreement between EP and CFD results is better in H cases, except for the lowest value of v_{10} for which T cases show a better agreement.

Figure 12 shows Q results for CV-H cases. EP reproduces the CFD value of Q for $v_{10} \geq 1.0$ m/s with a difference of less than 12 % and 13 %, for $v_{10} = 0.5$ m/s the difference is less than 15 % and 13 %, but for $v_{10} = 0.1$ m/s and 750 W the difference is up to 472 % and 449 %. For UCV-H cases, the difference between EP and CFD Q results for $v_{10} \geq 3.0$ m/s is less than 51 % and 1 %, for $v_{10} = 1.0$ m/s is up to 81 % and 22 %, for $v_{10} = 0.5$ m/s is up to 187 % and 95 %, and for $v_{10} = 0.1$ m/s is up to 1,240 % and 788 %. For the CV configuration the results using C1

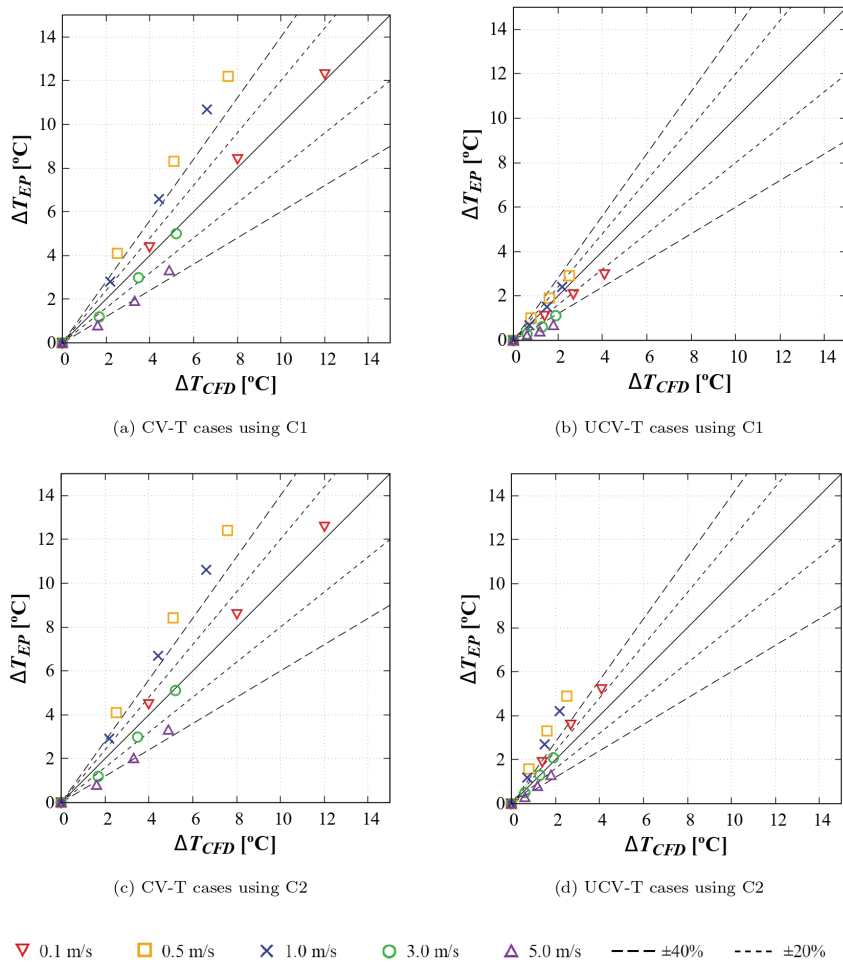


Figure 11. Comparison of ΔT from EnergyPlus and CFD simulations for T-cases, and for different wind speeds and heat levels, a) and b) using C1, c) and d) using C2. Symbols denote the wind speed at a 10 m height. For a given v_{10} the four heat levels can be distinguished since the values of ΔT and Q increase with the increase of the heat flux or the temperature on the floor. The dashed lines indicate the error in percentage

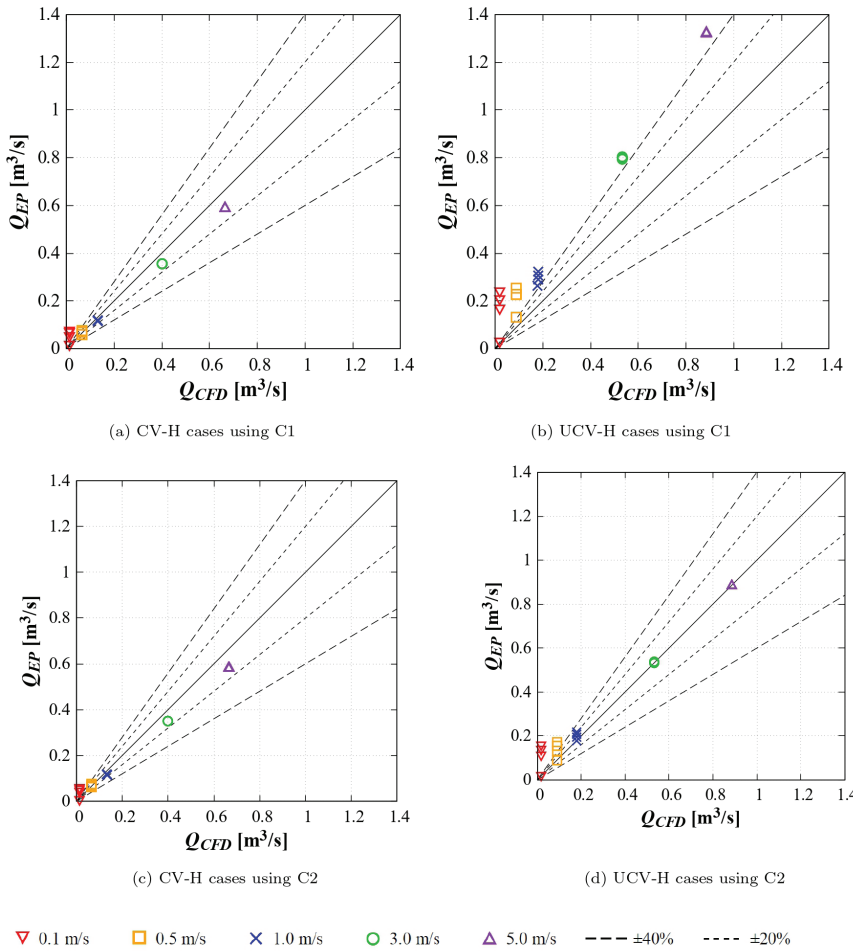


Figure 12. Comparison of Q from EnergyPlus and CFD simulations for H cases with different wind speeds and heat levels. a) and b) using C1, c) and d) using C2. Symbols denote wind speed at a 10 m height. For a given v_{10} the four heat levels can be distinguished since the values of ΔT and Q increase with the increase of the heat flux or the temperature on the floor. The dashed lines indicate the error in percentage

and C2 are similar, but for the UCV configuration the results improve significantly when C2 is used, especially for $v_{10} \geq 1.0$ m/s. Furthermore, when using Q as the comparison variable, the agreement between EP and CFD is better for the CV configuration than it is for the UCV.

Figure 13 shows Q results for CV-T cases. EP reproduces the CFD value of Q for $v_{10} \geq 1.0$ m/s with a difference of less than 13 % and 14 %, for $v_{10} = 0.5$ m/s the difference is up to 40 % and 35 %, for $v_{10} = 0.1$ m/s the difference is up to 601 % and 569 %. For the UCV-T cases, the difference between EP and CFD Q results for $v_{10} \geq 3.0$ m/s is less than 52 % and 2 %, for $v_{10} = 1.0$ m/s is up to 99 % and 34 %, for $v_{10} = 0.5$ m/s is up to 234 % and 121 %, and for $v_{10} = 0.1$ m/s is up to 1,515 % and 944 %. For the CV configuration, as in the H cases, the results using C1 and C2 are similar, while for the UCV configuration, the results improve significantly when C2 is used, especially for $v_{10} \geq 1.0$ m/s.

When using Q to compare the H and T cases, the agreement between EP and CFD results is slightly better for H cases. This improvement is more noticeable for $v_{10} \leq 0.5$ m/s. In both types of cases (H and T), for $v_{10} \leq 0.5$ m/s the difference between EP and CFD Q values increases as the heat level increases. For these values of v_{10} , EP overestimates Q with respect to the CFD. This overestimation is larger for the UCV configuration.

In general, EP gives better results for ΔT than it does for Q , especially for the CV configuration and the H cases.

One of the reasons for the difference in results between EP and CFD could be related to the fact that EP only predicts one or two values of T_i for the entire thermal zone, while CFD calculates the T_i value for each cell. To analyze this hypothesis the spatial average of T_i (\bar{T}_i) and the percentage difference of Q are plotted as functions of the difference between the maximum and the average indoor temperatures obtained from the CFD simulations ($\Delta T_{iCFD} = T_{maxCFD} - \bar{T}_{iCFD}$).

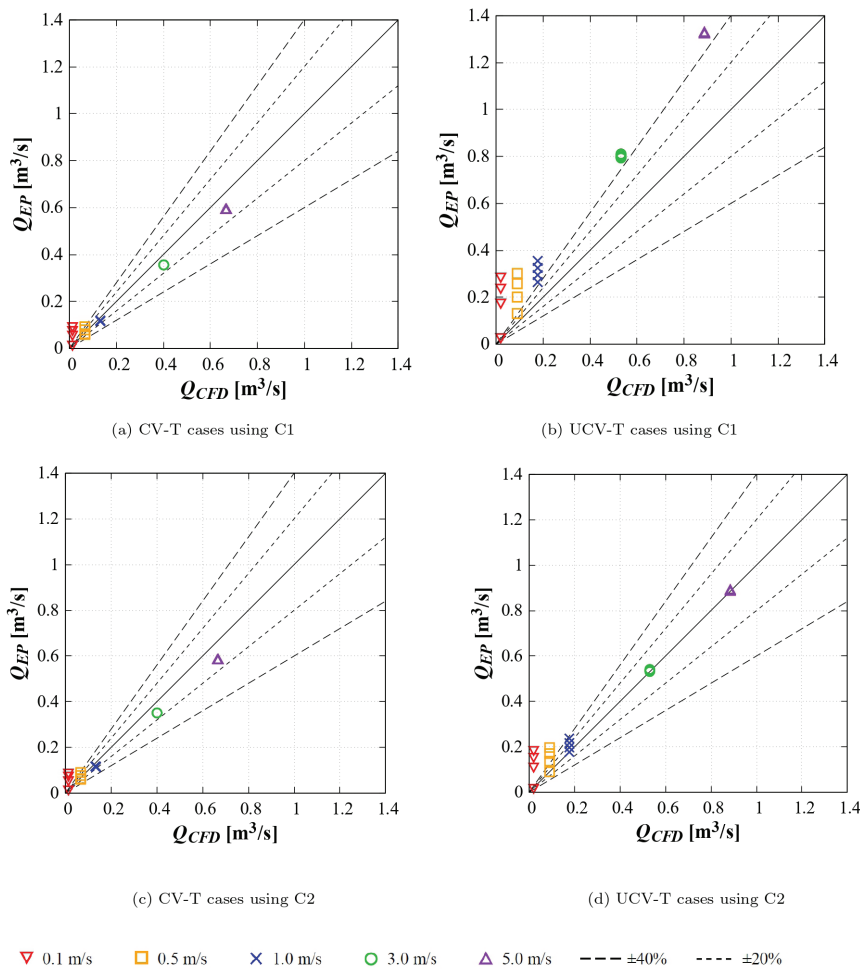


Figure 13. Comparison of Q from EnergyPlus and CFD simulations for H cases with different wind speeds and heat levels. a) and b) using C1, c) and d) using C2. Symbols denote wind speed at a 10 m height. For a given v_{10} the four heat levels can be distinguished since the values of ΔT and Q increase with the increase of the heat flux or the temperature on the floor. The dashed lines indicate the error in percentage

Figure 14 shows the difference for \bar{T}_i between EP results (using C1) and CFD results ($\delta \bar{T}_i = \bar{T}_{iEP} - \bar{T}_{iCFD}$) as a function of ΔT_{iCFD} . As expected, it can be observed that for all cases $\delta \bar{T}_i$ increases with the increase of ΔT_{iCFD} . The values of ΔT_{iCFD} are larger for H cases than they are for T cases. They also show the larger $\delta \bar{T}_i$ of up to 50°C. For H cases the value for $\delta \bar{T}_i$ is always negative, meaning that \bar{T}_i from EP is smaller than the value obtained from CFD.

For T cases the values of $\delta \bar{T}_i$ are larger for CV cases than for UCV cases. For CV cases $\delta \bar{T}_i$ is up to 5°C and for UCV cases it is up to 1°C.

Figure 15 shows the percentage difference for Q between EP using C1 and CFD simulations ($\delta Q = (Q_{EP} - Q_{CFD})/Q_{CFD}$) as a function of ΔT_{iCFD} . In all cases δQ increases as ΔT_{iCFD} increases. The values of ΔT_{iCFD} and δQ are larger for H cases than they are for T cases. H cases show values of δQ of up to 1,300 %.

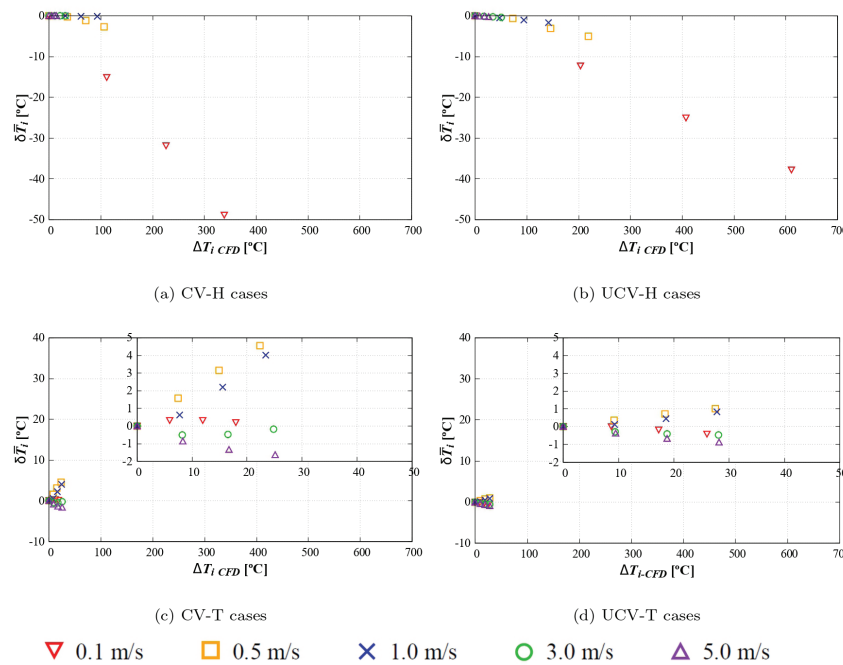


Figure 14. Difference in the average indoor temperatures from EnergyPlus (using C1) and CFD ($\delta \bar{T}_i$) as a function of the difference of the maximum and average indoor temperatures obtained from CFD ($\Delta T_{i,CFD}$) for different wind speeds (v_{10}) and heat levels. a) CV-H cases, b) UCV-H cases, c) CV-F cases, and (d) UCV-F cases. Symbols denote wind speed at a 10 m height. Note that the scales for ($\delta \bar{T}_i$) are different for the H and T cases, but the ranges are the same (50°C)

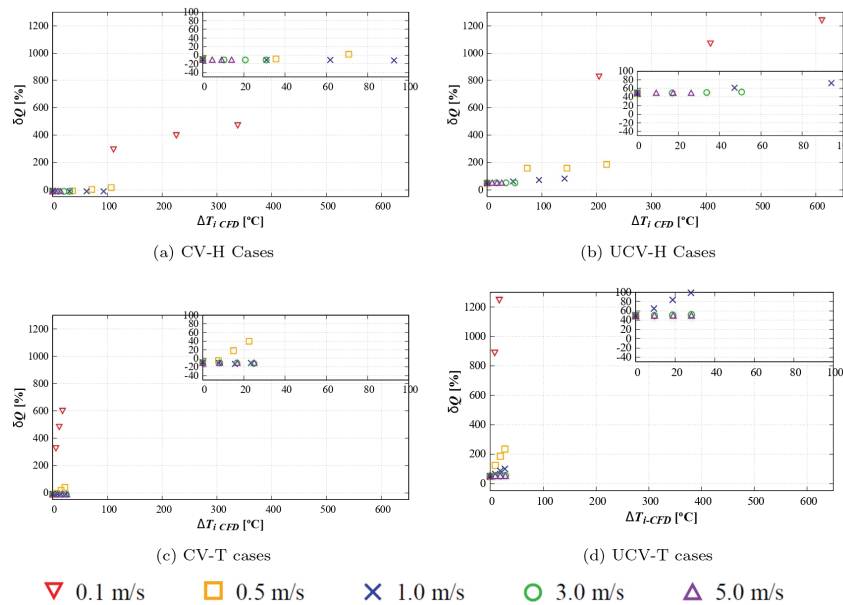


Figure 15. Percentage difference in the airflow rate Q from EnergyPlus (using C1) and CFD (δQ) as a function of the difference between the maximum and average indoor temperatures obtained from CFD ($\Delta T_{i,CFD}$) for different wind speeds (v_{10}) and heat levels. a) CV-H cases, b) UCV-H cases, c) CV-F cases, and d) UCV-F cases. Symbols denote wind speed at a 10 m height

CONCLUSIONS

Results of natural ventilation cases obtained from EnergyPlus (EP) simulations using the Airflow Network model (AFN) and the cross-ventilation model are compared with results from validated computational fluid dynamic (CFD) simulations. All simulations are performed in a steady state. Wind and buoyancy effects are considered for two configurations: cross ventilation

(CV) and upward cross ventilation (UCV). The buoyancy effect is produced by two heating modes: fixing a constant heat flux through the floor (H) and fixing a constant floor temperature (T). For each heating mode, four heating levels are considered. Wind speed at a 10 m height (v_{10}) is varied from 0.1 m/s to 5.0 m/s. EP results using one of two coefficient groups (C1 and C2) are compared with results from the CFD simulations. In the C1 group, the wind induced pressure coefficients C_p

are calculated by EP, and the discharge coefficients C_d are taken from the literature. In the C2 group, these coefficients are obtained from the CFD simulations.

The main conclusions derived from this work are the following:

- It is important to use the EP cross-ventilation model for the CV and UCV configurations. Although the temperature difference between the recirculation region and the jet region is smaller than 0.4 °C, the percentage velocity difference between the jet region and the recirculation region with respect to the jet region is up to 42 %.
- In the CV configuration, EP using C1 predicts good results for indoor air temperature (T_i) and airflow rate (Q) in the following conditions: $v_{10} = 0.5$ m/s and floor temperature $\leq 25^\circ\text{C}$ or floor heat flux ≤ 250 W; $v_{10} = 1.0$ m/s and floor temperature $\leq 25^\circ\text{C}$ or all floor heat flux levels; and $v_{10} \geq 3.0$ m/s for all floor heat levels. EP predicts T_i with a difference of up to 1.6 °C and Q with a difference of up to 12 % with respect to CFD simulations.
- In the UCV configuration, EP using C1 only predicts good results for T_i in the following conditions: $v_{10} = 0.5$ m/s without heating; $v_{10} = 1.0$ m/s and all floor temperatures or floor heat flux ≤ 250 W; and $v_{10} \geq 3.0$ m/s for all heat levels. EP predicts T_i with a difference of up to 1.0 °C with respect to CFD simulations. EP overestimates Q with respect to CFD simulations. This difference is up to 52 % for all velocities without heating as well as for $v_{10} \geq 3.0$ m/s for all heat levels.
- In the CV configuration, EP using C2 coefficients gives similar results to those obtained using C1 coefficients. In contrast, the use of C2 coefficients for the UCV configuration significantly improves results, particularly for Q .
- In the UCV configuration, EP using C2 coefficients predicts very good results (T_i with a difference up to 0.5 °C and Q with a difference up to 3 % with respect to CFD simulations) in the following conditions: all velocities without heating and $v_{10} \geq 3.0$ m/s for all heat levels. EP gives satisfactory results (the differences with respect to CFD simulations are up to 2 °C for T_i and up to 34 % for Q) for the cases with $v_{10} = 1.0$ m/s and all heat levels.

Thus, for the UCV configuration it is recommended to use coefficients obtained from CFD simulations, instead of the C_p calculated by EP and the C_d taken from the literature.

It is recommended that the Airflow Network model be employed for practical thermal simulations of natu-

rally ventilated buildings using EnergyPlus (EP). The cross-ventilation model must also be used for thermal zones with cross-ventilation.

The analyses made in this research show that an improvement on the natural ventilation models of EP is required, especially for low wind velocity and high heat internal gain conditions. The authors are beginning experimental and theoretical research on thermally driven natural ventilation (Castillo *et al.*, 2021), and they expected to make a model to be incorporated in EP in the near future.

NOMENCLATURE

Acronyms

AFN	Airflow Network Model
AIVC	Air Infiltration and Ventilation Centre
CFD	Computational Fluid Dynamics
CV	Cross Ventilation
EP	EnergyPlus
NNV	Natural Night Ventilation
PIV	Particle Image Velocimetry
SPIV	Stereoscopic Particle Image Velocimetry
TARP	Thermal Analysis Research Program
UCV	Upward Cross Ventilation
WE	Windexchanger

Latin symbols

A_{CH}	Air changes per hour [1/h]
C_d	Discharge coefficient [-]
C_p	Pressure coefficient [-]
k	Turbulent kinetic energy [m^2/s^2]
k_s	Sand grain roughness height [m]
Q	Air flow rate [m^3/s]
q	Heat flow rate [W]
T_i	Indoor air temperature [°C]
T_o	Outdoor air temperature [°C]
u	Air velocity (or water velocity) [m/s]
u_{ABL}^*	Atmospheric boundary layer friction velocity [m/s]
U_{ref}	Reference velocity equal to the wind velocity at the building height [m/s]
u_{ref}	Reference velocity equal to the wind velocity at the opening height [m/s]
v_{10}	Wind speed at a 10 m height [m/s]
z_0	Roughness length [m]

Greek symbols

ΔT	Temperature difference between the indoor and outdoor air [°C]
ω	Specific dissipation rate [1/s]

ACKNOWLEDGMENTS

Authors thank the technical support provided by Margarita Pedraza, Héctor Cortés and Alfredo Quiroz. This work was partially supported by the IN109519 and IT101824 project sponsored by PAPIIT-UNAM. M.V. Cruz-Salas (CVU 422473) acknowledges the postdoctoral fellowship granted by CONACYT.

REFERENCES

- Albuquerque, D. P., Mateus, N., Avantaggiato, M., & Carrilho da Graça, G. (2020). Full-scale measurement and validated simulation of cooling load reduction due to nighttime natural ventilation of a large atrium. *Energy and Buildings*, 224, 110233. <https://doi.org/10.1016/j.enbuild.2020.110233>
- Andelković, A. S., Mujan, I., & Dakić, S. (2016). Experimental validation of a energyplus model: Application of a multi-storey naturally ventilated double skin façade. *Energy and Buildings*, 118, 27-36. <https://doi.org/10.1016/j.enbuild.2016.02.045>
- ANSYS. (2018). *Fluent 19 user's guide*. Lebanon: Fluent Inc.
- Arendt, K., Krzaczek, M., & Tejchman, J. (2017). Influence of input data on airflow network accuracy in residential buildings with natural wind- and stack-driven ventilation. *Building Simulation*, 10(2), 229-238. <https://doi.org/10.1007/s12273-016-0320-5>
- ASHRAE. (2013). *Handbook Fundamentals, SI edn*. Atlanta, USA: American Society of Heating, Refrigerating and Air Conditioning Engineers (ASHRAE).
- Belleri, A., Lollini, R., & Dutton, S. M. (2014). Natural ventilation design: An analysis of predicted and measured performance. *Building and Environment*, 81, 123-138. <https://doi.org/10.1016/j.buildenv.2014.06.009>
- Blocken, B. (2015). Computational fluid dynamics for urban physics: Importance, scales, possibilities, limitations and ten tips and tricks towards accurate and reliable simulations. *Building and Environment*, 91, 219245. <https://doi.org/10.1016/j.buildenv.2015.02.015>
- Blocken, B., Stathopoulos, T., & Carmeliet, J. (2007). CFD simulation of the atmospheric boundary layer: wall function problems. *Atmospheric Environment*, 41(2), 238-252. <https://doi.org/10.1016/j.atmosenv.2006.08.019>
- Castillo, J. A. & Huelsz, G. (2017). A methodology to evaluate the indoor natural ventilation in hot climates: Heat Balance Index. *Building and Environment*, 114, 366-373. <https://doi.org/10.1016/j.buildenv.2016.12.027>
- Castillo, J. A., Cruz-Salas, M. V., & Huelsz, G. (2017). Natural ventilation by windexchangers in a building with a window in prevailing winds: design guidelines. *International Journal of Ventilation*, 16, 1-14. <https://doi.org/10.1080/14733315.2016.1252145>
- Castillo, J. A., Huelsz, G., van Hooff, T., & Blocken, B. (2019). Natural ventilation of an isolated generic building with a windward window and different windexchangers: CDF validation, sensitivity study and performance analysis. *Building Simulation*, 12(3), 475-488. <https://doi.org/10.1007/s12273-018-0502-4>
- Castillo, J. A., Tovar, R., & Huelsz, G. (2021). Natural ventilation in a room with a horizontal cylindrical heat source, a window and bottom or top vents. *Building and Environment*, 191, 107583. <https://doi.org/10.1016/j.buildenv.2020.107583>
- Cebeci, T. & Bradshaw, P. (1977). *Momentum transfer in boundary layers*. Schaum's Solved Problems. Hemisphere Publishing Corporation. ISBN 9780070103009.
- Chan, A.L.S., Chow, T. T., Fong, K. F., & Lin, Z. (2009). Investigation on energy performance of double skin façade in Hong Kong. *Energy and Buildings*, 41(11), 1135-1142. <https://doi.org/10.1016/j.enbuild.2009.05.012>
- Cheng, X., Zhang, H., Pan, W., Liu, S., Zhang, M., Long, Z., Zhang, T., & Chen, Q. (2017). Field study of infiltration rate and its influence on indoor air quality in an apartment. *Procedia Engineering*, 205, 3954-3961. <https://doi.org/10.1016/j.proeng.2017.09.853>
- Choi, W., Joe, J., Kwak, Y., & Huh, J.-H. (2012). Operation and control strategies for multistorey double skin façades during the heating season. *Energy and Buildings*, 49, 454-465. <https://doi.org/10.1016/j.enbuild.2012.02.047>
- Chu, C.-R. (2023). Assessment of year-round wind-driven ventilation by an integrated ventilation model. *Building and Environment*, 243, 110710. <https://doi.org/10.1016/j.buildenv.2023.110710>
- Cruz-Salas, M. V., Castillo, J. A., & Huelsz, G. (2014). Experimental study on natural ventilation of a room with a windward window and different windexchangers. *Energy and Building*, 84, 458-465. <https://doi.org/10.1016/j.enbuild.2014.08.033>
- DOE. (2016). *EnergyPlus v. 8.7 Documentation*. Engineering Reference. U.S. Department of Energy, DOE.
- Dogan, T. & Kastner, P. (2021). Streamlined CFD simulation framework to generate windpressure coefficients on building facades for airflow network simulations. *Building Simulation*, 14(4), 1189-1200. <https://doi.org/10.1007/s12273-020-0727-x>
- Fouquier, A., Robert, S., Suard, F., Stéphan, L., & Jay, A. (2013). State of the art in building modelling and energy performances prediction: A review. *Renewable and Sustainable Energy Reviews*, 23, 272-288. <https://doi.org/10.1016/j.rser.2013.03.004>
- Franke, J., Hellsten, A., Schlünzen, H., & Carissimo, B. (2007). The COST 732 Best Practice Guideline for CFD simulation of flows in the urban environment: a summary. *International Journal of Environment and Pollution*, 44, 1-4. <https://doi.org/10.1504/IJEP.2011.038443>
- Gallardo, J. P., Pettersen, B., & Andersson, H. I. (2013). Effects of free-slip boundary conditions on the flow around a curved circular cylinder. *Computers & Fluids*, 86, 389-394. <https://doi.org/10.1016/j.compfluid.2013.07.023>
- Gilani, S., Montazeri, H., & Blocken, B. (2016). CDF simulation of stratified indoor environment in displacement ventilation:

- Validation and sensitivity analysis. *Building and Environment*, 95, 299-313. <https://doi.org/10.1016/j.buildenv.2015.09.010>
- Gimenez, J. M., Bre, F., Nigro, N. M., & Fachinotti, V. (2018). Computational modeling of natural ventilation in low-rise nonrectangular floor-plan buildings. *Building Simulation*, 11, 1255-1271. <https://doi.org/10.1007/s12273-018-0461-9>
- Goncalves, V. L., Costanzo, V., Fabbri, K., & Rakha, T. (2022). Overheating assessment in passivhaus dwellings: the influence of prediction tools. *Buildings and Cities*, 3(1), 153-167. <https://doi.org/10.5334/bc.151>
- Hashemi, N., Fayaz, R., & Sarsha, M. (2010). Thermal behaviour of a ventilated double skin façade in hot arid climate. *Energy and Buildings*, 42(10), 1823-1832. <https://doi.org/10.1016/j.enbuild.2010.05.019>
- Heiselberg, P., Svidt, K., & Nielsen, P. V. (2001). Characteristics of airflow from open windows. *Building and Environment*, 36(7), 859-869. [https://doi.org/10.1016/S0360-1323\(01\)00012-9](https://doi.org/10.1016/S0360-1323(01)00012-9)
- Joe, J., Choi, W., Kwon, H., & Huh, J.-H. (2013). Load characteristics and operation strategies of building integrated with multi-story double skin facade. *Energy and Buildings*, 60, 185-198. <https://doi.org/10.1016/j.enbuild.2013.01.015>
- Karava, P., Stathopoulos, T., & Athienitis, A. K. (2004). Natural ventilation openings a discussion of discharge coefficients, building for the future: The 16th cib world building congress, in-house publishing, Rotterdam, Netherlands.
- Kobayashi, T., Sandberg, M., Fujita, T., Lim, E., & Umemiya, N. (2022). Numerical analysis of wind-induced natural ventilation for an isolated cubic room with two openings under small mean wind pressure difference. *Building and Environment*, 226, 109694. <https://doi.org/10.1016/j.buildenv.2022.109694>
- Kosutova, K., van Hooff, T., & Blocken, B. (2018). CFD simulation of non-isothermal mixing ventilation in a generic enclosure: Impact of computational and physical parameters. *International Journal of Thermal Sciences*, 129, 343-357. <https://doi.org/10.1016/j.ijthermalsci.2018.03.001>
- Kosutova, K., van Hooff, T., Vanderwel, C., Blocken, B., & Hensen, J. (2019). Crossventilation in a generic isolated building equipped with louvers: Wind-tunnel experiments and CFD simulations. *Building and Environment*, 154, 263-280. <https://doi.org/10.1016/j.buildenv.2019.03.019>
- Kumar, N., Kubota, T., Tominaga, Y., Shirzadi, M., & Bardhan, R. (2021). CFD simulations of wind-induced ventilation in apartment buildings with vertical voids: Effects of pilotis and wind fin on ventilation performance. *Building and Environment*, 194, 107666. <https://doi.org/10.1016/j.buildenv.2021.107666>
- Kurabuchi, T., Ohba, M., Endo, T., Akamine, Y., & Nakayama, F. (2004). Local dynamic similarity model of cross-ventilation part 1-theoretical framework. *International Journal of Ventilation*, 2, 371-382. <https://doi.org/10.1080/14733315.2004.11683679>
- Le, S., Chen, Y., Bi, Y., & Lu, X. (2014). Modeling and simulation of ventilated double-skin façade using energyplus. In Proceedings of the 8th International Symposium on Heating, Ventilation and Air Conditioning. Lecture Notes in Electrical Engineering, 3, 241-252.
- Li, C. & Chen, Y. (2023). A multi-factor optimization method based on thermal comfort for building energy performance with natural ventilation. *Energy and Buildings*, 285, 112893. <https://doi.org/10.1016/j.enbuild.2023.112893>
- Linden, P. F., Lane-Serff, G. F., & Smeed, D. A. (1990). Emptying filling boxes: The fluid mechanics of natural ventilation. *Journal of Fluid Mechanics*, 212, 309-335. <https://doi.org/10.1017/S0022112090001987>
- Lishman, B. & Woods, A. W. (2006). The control of naturally ventilated buildings subject to wind and buoyancy. *Journal of Fluid Mechanics*, 557, 451-471. <https://doi.org/10.1017/S0022112006009931>
- Lu, Y., Dong, J., & Liu, J. (2020). Zonal modelling for thermal and energy performance of large space buildings: A review. *Renewable and Sustainable Energy Reviews*, 133, 110241. <https://doi.org/10.1016/j.rser.2020.110241>
- Ohba, M. & Lun, I. (2010). Overview of natural cross-ventilation studies and the latest simulation design tools used in building ventilation-related research. *Advances in Building Energy Research*, 4(1), 127-166. <https://doi.org/10.3763/aber.2009.0405>
- Peng, J., Curcija, D. C., Lu, L., Selkowitz, S. E., Yang, H., & Mitchell, R. (2016). Developing a method and simulation model for evaluating the overall energy performance of a ventilated semi-transparent photovoltaic double-skin façade. *Progress in Photovoltaics: Research and Applications*, 24(6), 781-799. <https://doi.org/10.1002/pip.2727>
- Peren, J. I., van Hooff, T., Ramponi, R., Blocken, B., & Leite, B. C. C. (2015). Impact of roof geometry of an isolated leeward sawtooth roof building on cross-ventilation: Straight, concave, hybrid or convex? *Journal of Wind Engineering and Industrial Aerodynamics*, 145, 102-114. <https://doi.org/10.1016/j.jweia.2015.05.014>
- Perén, J. I., van Hooff, T., Leite, B. C.C., & Blocken, B. (2015). Impact of eaves on cross-ventilation of a generic isolated leeward sawtooth roof building: Windward eaves, leeward eaves and eaves inclination. *Building and Environment*, 92, 578-590. <https://doi.org/10.1016/j.buildenv.2015.05.011>
- Ramponi, R. & Blocken, B. (2012). CFD simulation of cross-ventilation for a generic isolated building: Impact of computational parameters. *Building and Environment*, 53, 34-48. <https://doi.org/10.1016/j.buildenv.2012.01.004>
- Ramponi, R., Gaetani, I., & Angelotti, A. (2014). Influence of the urban environment on the effectiveness of natural night-ventilation of an office building. *Energy and Buildings*, 78, 25-34. <https://doi.org/10.1016/j.enbuild.2014.04.001>
- Rusly, E. & Piechowski, M. (2011). Impacts of infiltration/exfiltration from wind, stack and buoyancy in a/c design-An energy-plus simulation case study. In Proceedings of Building Simulation 2011: 12th Conference of International Building Performance Simulation Association, 823-830.

- Sakiyama, N. R. M., Carlo, J. C., Sakiyama, F. I. H., Abdessemed, N., Frick, J., & Garrecht, H. (2024). Impact of wind pressure coefficients on the natural ventilation effectiveness of buildings through simulations. *Buildings*, 14, 2803. <https://doi.org/10.3390/buildings14092803>
- Salvati, A. & Kolokotroni, M. (2023). Urban microclimate and climate change impact on the thermal performance and ventilation of multi-family residential buildings. *Energy and Buildings*, 294, 113224. <https://doi.org/10.1016/j.enbuild.2023.113224>
- Schulze, T. & Eicker, U. (2013). Controlled natural ventilation for energy efficient buildings. *Energy and Buildings*, 56, 221-232. <https://doi.org/10.1016/j.enbuild.2012.07.044>
- Shirzadi, M., Mirzaei, P. A., & Naghashzadegan, M. (2018). Development of an adaptive discharge coefficient to improve the accuracy of cross-ventilation airflow calculation in building energy simulation tools. *Building and Environment*, 127, 277-290. <https://doi.org/10.1016/j.buildenv.2017.10.019>
- Sung, U. J., Cho, S., Seo, D. H., & Song, K. D. (2013). Analysis of reduced cooling load for a multistorey-building incorporating a ventilated double skin façade with a solar chimney channel. *International Journal of Ventilation*, 11(4), 381-392. <https://doi.org/10.1080/14733315.2013.11683995>
- Tan, G. & Glicksman, L. R. (2005). Application of integrating multi-zone model with CDF simulation to natural ventilation prediction. *Energy and Buildings*, 37(10), 1049-057. <https://doi.org/10.1016/j.enbuild.2004.12.009>
- Tominaga, Y., Mochida, A., Yoshie, R., Kataoka, H., Nozu, T., Yoshikawa, M., & Shirasawa, T. (2008). AIJ guidelines for practical applications of CFD to pedestrian wind environment around buildings. *Journal of Wind Engineering and Industrial Aerodynamics*, 96(10-11), 1749-1761. <https://doi.org/10.1016/j.jweia.2008.02.058>
- van Hooff, T. & Blocken, B. (2010). Coupled urban wind flow and indoor natural ventilation modelling on a high-resolution grid: A case study for the Amsterdam Arena stadium. *Environmental Modelling and Software*, 25(1), 51-65. <https://doi.org/10.1016/j.envsoft.2009.07.008>
- van Hooff, T., Blocken, B., & Tominaga, Y. (2017). On the accuracy of CDF simulations of cross-ventilation flows for a generic isolated building: Comparison of RANS, LES and experiments. *Building and Environment*, 114, 148-165. <https://doi.org/10.1016/j.buildenv.2016.12.019>
- Xie, X., Luo, Z., Grimmond, S., & Blunn, L. (2023). Use of wind pressure coefficients to simulate natural ventilation and building energy for isolated and surrounded buildings. *Building and Environment*. 230, 109951. <https://doi.org/10.1016/j.buildenv.2022.109951>
- Yan, B., Malkawi, A., & Chen, Y. (2015). A method for estimating cooling energy savings potential from using mixed-mode ventilation. In 14th International Conference of IBPSA - Building Simulation 2015, BS 2015, Conference Proceedings, 782-789.
- Yin, X. & Muhiedeen, M. W. (2024). Evaluation of cooling energy saving and ventilation renovations in office buildings by combining bioclimatic design strategies with CFD-BEM coupled simulation. *Journal of Building Engineering*, 91, 109547. <https://doi.org/10.1016/j.jobe.2024.109547>
- Zhai, Z. J., Johnson, M.-H., & Krarti, M. (2011). Assessment of natural and hybrid ventilation models in whole-building energy simulations. *Energy and Buildings*, 43(9), 2251-2261. <https://doi.org/10.1016/j.enbuild.2011.06.026>
- Zhang, R., Lam, K. P., Yao, S., & Zhang, Y. (2013). Coupled EnergyPlus and computational fluid dynamics simulation for natural ventilation. *Building and Environment*, 68, 100-113. <https://doi.org/10.1016/j.buildenv.2013.04.002>
- Zheng, X., Montazeri, H., & Blocken, B. (2020). CFD simulations of wind flow and mean surface pressure for buildings with balconies: Comparison of RANS and LES. *Building and Environment*, 173, 106747. <https://doi.org/10.1016/j.buildenv.2020.106747>

Cómo citar:

Cruz-Salas, M. V., Castillo, J. A., & Huelsz, G. (2025). EnergyPlus simulations of naturally ventilated buildings: comparison with validated CFD simulations. *Ingeniería Investigación y Tecnología*, 26(01), 1-18. <https://doi.org/10.22201/fi.25940732e.2025.26.1.006>